ELSEVIER

Journal of Chromatography A, 776 (1997) 179–195

JOURNAL OF CHROMATOGRAPHY A

Fluidization characteristics of and protein adsorption on fluoride-modified porous zirconium oxide particles

C.M. Griffith[c], J. Morris[d], M. Robichaud[d], M.J. Annen[b,c], A.V. McCormick[c], M.C. Flickinger[a,d,*]

[a]*Department of Biochemistry, Biological Process Technology Institute, University of Minnesota, St. Paul, MN 55108-6106, USA*
[b]*Department of Chemistry, Biological Process Technology Institute, University of Minnesota, Minneapolis, MN 55455-6106, USA*
[c]*Department of Chemical Engineering and Materials Science, Biological Process Technology Institute, University of Minnesota, Minneapolis, MN 55455-6106, USA*
[d]*Biological Process Technology Institute, University of Minnesota, St. Paul MN 55108-6106, USA*

Received 26 January 1996; revised 11 March 1997; accepted 11 March 1997

Abstract

Porous zirconia particles of specific gravity ~3.2 g/ml, mean particle sizes of ~50 μm, and terminal settling velocity of ~2.8 mm/s in water, were synthesized using an oil emulsion method from 1000 Å colloids and were evaluated for their potential use in expanded bed protein adsorption. Expanded beds of particles were stable even for small volume, shallow beds (settled bed: 10 ml, height to diameter ratio <1.0) and even for fluidization velocities common to much larger particles (210 cm/h for a three-fold bed expansion). When the surface of these particles was modified by fluoride adsorption, the total bed capacity for bovine serum albumin (BSA) adsorption was 42±2 mg BSA/ml of settled bed volume at linear velocities of 109–210 cm/h. Residence time distribution studies of several solutes under non-binding conditions were performed to assess the degree of liquid mixing and channeling in the expanded bed as a function of fluidization velocity. Liquid mixing and channeling were also studied as a function of distributor design. With these very dense particles, the degree of channeling and mixing did not worsen with the degree of expansion. Elution of adsorbed BSA while the bed was expanded (by a step increase in ionic strength) was rapid resulting in a narrow peak at high fluidization velocities without resorting to settling of the bed. The dynamic binding capacity of BSA at 5% breakthrough (protein effluent concentration equal to 5% of the inlet concentration) was the same for a two-fold expanded bed as for a settled bed (22±2 mg BSA/ml of settled bed volume), though it decreased for higher bed expansions. BSA binding was reproducible following repeated cleaning of the adsorbent with 0.25 *M* sodium hydroxide.

Keywords: Zirconia; Fluoride-modified zirconia; Adsorbents; Stationary phases, LC; Proteins; Albumin

1. Introduction

The advantages of expanded beds of ion-exchange [1–5] or affinity adsorbents [6–13] for adsorption of proteins from biological process liquids have been recently reviewed [9,14]. Prior to this report, fluidized-bed batch protein adsorption studies investigated 100–400 μm polymeric, silica or composite particles with high settled bed height to diameter and only a small density difference between adsorbent particles and process fluids. Both the particle physical characteristics (size, density, shape) and the

*Corresponding author.

0021-9673/97/$17.00
PII S0021-9673(97)00282-3

mixing characteristics of the expanded bed are important for efficient protein adsorption [14]. Large silica and polymeric particles have a long characteristic diffusion length within the adsorbent. Moreover, they are unable to be repeatedly cleaned with harsh reagents [9,14].

The ability to repeatedly remove non-specifically adsorbed protein, nucleic acids, lipids, pyrogenic lipopolysaccharides (LPSs), and contaminating viruses or microorganisms from chromatographic media is a challenging problem in the separation of proteins for therapeutic use [22–33]. Harsh cleaning methods are needed to remove and inactivate lipopolysaccharide endotoxin (LPS) and viral nucleic acids [24,26–33] from protein adsorbent media because of federal and World Health Organization regulations for human biology [34,35]. Therefore, both the adsorbent surface and ligand need to be stable to repeated clean-in-place cycles without loss of capacity or mechanical stability. Some silica-coated and polymeric adsorbents tolerate cleaning with 0.1 *M* sodium hydroxide or ethanol–acetic acid mixtures and are more mechanically stable than carbohydrate adsorbents [36,37]. In general, polymeric adsorbents cannot be sterilized with heat and silica adsorbents cannot be sanitized with 0.2–1.0 *M* sodium hydroxide without degradation.

One approach to improve expanded bed protein adsorption is to develop porous stable adsorbent particles of high density. With very dense particles, high fluidization velocities (100–250 cm/h) can be achieved with smaller adsorbent particles resulting in more rapid protein adsorption [10,16,17]. The use of dense particles should also result in a stable expanded bed over a wider range of fluid densities and viscosities with reduced dispersion within the bed and may achieve higher throughput than packed bed chromatography [4,9–12]. Recently, titanium composite, surface-modified glass particles and perfluoropolymer affinity adsorbents [13] of densities as high as 2.2 g/ml [11,12] have been evaluated as protein adsorbents at high flow-rates and bed heights [14–18].

Porous particles (d_p=4–20 μm) of zirconium oxide have recently been developed [19–21]. The surface of these amphoteric metal oxide particles is dominated by Lewis acid sites which when not inhibited by hard Lewis bases in the mobile phase, irreversibly adsorb proteins. With suitable surface modifications which are stable to strong cleaning agents (e.g., sodium hydroxide) or can easily be regenerated, larger and more dense porous zirconium oxide particles (50–150 μm, 3.2 g/ml) are potentially useful for purification of proteins where the adsorbent needs to be repeatedly cleaned with sodium hydroxide or steam.

In this work, small quantities of large, surface-modified porous zirconium oxide particles were synthesized and evaluated for their use in expanded bed protein adsorption using a shallow bed (settled bed height to diameter of approximately 1.0). The fluidization properties and protein adsorption capacity of these particles were examined in a model small diameter column which allowed rapid evaluation of particles synthesized using a laboratory scale oil emulsion process.

Bare zirconia binds proteins irreversibly [19–21] and therefore a base stable, easily regeneratable modification of the zirconium oxide surface by fluoride adsorption [38] is used which creates a strong cation and ligand exchange adsorbent. Bovine serum albumin (BSA) (Fraction V, Sigma, St. Louis, MO, USA) is used in order to determine protein adsorption during fluidization and to compare the characteristics of fluoride-adsorbed zirconia particles with studies of BSA adsorption using fluidized, polymeric ion-exchange adsorbents [2–5,9]. Ion-exchange adsorbents are unlikely to be used in direct recovery of many proteins from fermentation broths or cell culture fluids due to the high ionic strength of these fluids [28,39,40] and it is known that BSA is far from an ideal protein because of its non-specific adherance to column matrices. However, BSA adsorption by fluoride-modified zirconia is used here as a model system to determine fluidization characteristics and protein adsorption efficiency.

2. Experimental

2.1. Synthesis, classification and characterization of porous zirconium oxide particles

Porous zirconia particles were synthesized using a batch surfactant oil emulsion process [41–43]. A sol of nominally 1000 Å diameter zirconium oxide

colloid (Nyacol Lot 1V-40, Ashland, MA, USA) was centrifuged for 2 h at 1590 *g* (3000 rpm, Beckman JA 10 rotor, Fullerton, CA, USA) to remove colloids much smaller than the nominal diameter. Colloid batches of 80 g were resuspended by shaking at pH 3 in nitric acid solution to obtain a colloidal sol of approximately 16% (w/w). A volume of 1200 ml of peanut oil (Sigma) and 1200 ml of oleyl alcohol (Eastern Chemical, Hauppauge, NY, USA) were mixed and preheated to 85°C in a 4 l polypropylene container (18.3 cm diameter) using two 3-blade propellers (45° pitch) at 450 rpm (lower propeller 10.5 cm diameter, upper propeller 7.6 cm diameter; lower propeller 2 cm above the bottom of the beaker; upper propeller 5 cm above lower propeller). A mass of 40 g of urea and 0.33 ml of non-ionic surfactant (Triton X-100, Rohm and Haas, Philadelphia, PA, USA) were dissolved in each batch of resuspended sol. The batch was then poured into the agitated, preheated oil and alcohol mixture with constant stirring to create the sol–oil emulsion. The emulsion was continuously heated and stirred for 4 h in order to dehydrate the sol droplets. During the drying process, the droplets densified, the colloid within the droplets flocculated, and the droplets solidified into stable aggregates. During drying, samples were taken and particle size was monitored using light microscopy (230×magnification). When particle breakage began to be observed, the agitation rate was reduced to 360 rpm. After the drying process was allowed to continue for 4 h, the bath was removed from the heat and the particles were allowed to settle for 5 min. The particles remaining suspended were then removed by decanting the oil–alcohol mixture. The settled particles were washed three times with 75–100 ml of hexane, then washed three times with 25–50 ml of isopropanol, and then dried using vacuum filtration to a free-flowing powder.

Particles were heated to remove volatiles and sintered in a programmed temperature oven (2 h at 375°C, 6 h at 750°C, 3 h at 900°C, 40°C/min temperature ramp). After cooling, the particles were washed with carbonate-free, double distilled water with sonication (Branson, 1200, Danbury, CT, USA) under vacuum for 15 min. The liquid was decanted and the particles washed in excess carbonate-free 0.5 *M* sodium hydroxide (Mallinkrodt, St. Louis, MO, USA) on a shaker table overnight. The supernatant was decanted, the particles were again rinsed with carbonate-free double distilled water. The particles were then washed with gentle rocking in excess carbonate-free 0.5 *M* nitric acid (EM Science, Gibbstown, NJ, USA) on a shaker overnight, rinsed with copious amounts of double distilled water, and dried under vacuum at 100°C for 8 h. The particles were then sonicated in double distilled water under vacuum and stored in double distilled water.

A size distribution of 20–140 μm with ~50 μm average particle diameter was achieved by settling the particles in double distilled water in a graduated cylinder (1 l) for 30 min followed by decanting the fines. Elutriation was performed by ascending fluidization either in a 30 cm×1 cm inside diameter (I.D.) (Ace Glass, Vineland, NJ, USA) or a 15 cm×2.5 cm I.D. (Kontes, Vineland, NJ) glass column at a flow-rate sufficient for three to four fold expansion of the original settled bed volume for at least 30 min. Following elutriation, particles were allowed to settle overnight and then the bed was progressively expanded to remove any remaining small particles. A stable bed expansion was the absence of visible bed boiling, fluid jetting, and the absence of elutriating fines.

Particle surface area and pore volume were determined by nitrogen BET adsorption and desorption [44,45] using a Micrometrics ASAP 2000 V3.00 (Norcross, GA, USA). The particle specific gravity (the effective particle density during fluidization) was calculated using pore volume sorptometry and using gravimetry (comparing masses of a packed bed in air and in water). The density of monoclinic zirconia is 5.7±0.1 g/ml [20]. Particle morphology was examined using scanning electron microscopy (SEM) (Hitachi 5-450, San Jose, CA, USA). SEM samples were prepared using Au/Pd sputtering at 15 μA in argon at $1.3 \cdot 10^{-4}$ Pa for 3 min.

2.2. Expanded bed methods

Expanded bed studies were performed using a 2.5×15 cm glass column (Kontes). The column volume was adjustable with the use of a PTFE hydraulic header fitted with a stainless steel screen (with 38 μm openings) at the top of the column. The flow distributor at the column entrance was modified from a PEEK end fitting (polyether ether ketone,

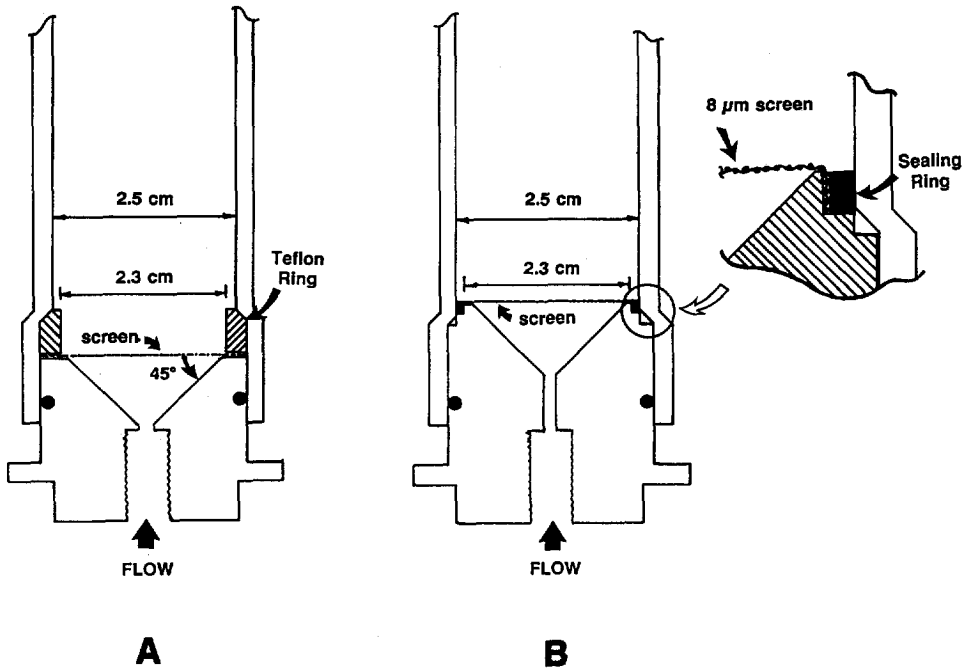

Fig. 1. Conical 45° flow distribution for ascending fluidization of porous zirconia particles (standard 4° flow distributor not shown). (A) Flat stainless steel screen secured with PTFE ring. (B) Stainless steel screen secured with sealing ring.

Fisher Scientific, Pittsburgh, PA, USA; Fig. 1) and fitted with an 8 μm, twilled dutch weave, stainless steel screen (Small Parts, Miami Lakes, FL, USA). The flow hydrodynamics of several column inlet flow distributor designs were evaluated: (1) an end fitting with a 45° cone and screen secured to the distributor with a PTFE sealing ring (Fig. 1A) (2) an end fitting with a standard 4° cone and screen secured to the distributor with a PTFE sealing ring (not shown, same configuration as Fig. 1A); and (3) an end fitting with a 45° cone and screen secured to the distributor with a flat neoprene binder ring and thin O-ring (Fig. 1B). The fluidized bed was connected to a peristaltic pump (Cole Parmer, Niles, IL, USA) using 0.8 mm I.D. PTFE tubing and tube fittings (Chrom Tech, Apple Valley, MN, USA). Either Tygon or Cflex tubing (Cole Parmer) was used in the peristaltic pump. A 316 stainless steel pressure gauge (ABM, Philadelphia, PA, USA) was attached to a three-way connector placed between the pump and the column inlet.

The concentration of the tracer in the column effluent was measured using a flow cell UV detector with a total cell volume of 30 μl (UV-M II Monitor, Pharmacia LKB Biotechnology, Uppsala, Sweden). The pH of the column effluent was measured using a pH meter (Orion Research, model 611, Cambridge, MA, USA). Settled bed height to column diameter ratio was 0.8:1.0 or 0.9:1.0. For all settled bed experiments, the hydraulic header was placed on top of the bed. For the expanded bed experiments, the hydraulic header was positioned either 1.00±0.05 cm or 0.10±0.05 cm above the bed surface.

The bed of particles was settled by successively tapping and shaking the column until the bed height did not change. The column was shaken and inverted to agitate the particles and then the particles were allowed to settle to ensure a consistent distribution and the column checked for vertical orientation at the start of each experiment.

The entire adsorption, washing, elution, and particle cleaning cycle was performed at a constant flow-rate. The only exception to this was when the pump was briefly turned off (approximately 4 s) when switching between the fluidizing solutions thereby preventing the creation of air bubbles in the

system tubing. When the pumping resumed, the volumetric flow-rate was gradually increased in a stepwise fashion over a period of 2.0–2.5 min until the appropriate flow-rate was achieved.

All solutions (except the solutions containing BSA) were filtered through a 0.22 μm filter (Gelman, Ann Arbor, MI, USA) and degassed by stirring under vacuum for several min. The BSA solutions were either made fresh at the start of each experiment or stored at 4°C for at most 3 days prior to use. The shear viscosities of all fluidizing solutions were measured at 22–23°C with a Rheometrics RFS-II (Piscataway, NJ, USA) shear rheometer using a Couette configuration [49].

2.3. Characterization of fluidization

The bed expansion characteristics of the zirconium oxide particles were determined using the correlation proposed by Richardson and Zaki [48], which relates the liquid superficial velocity, u, and the interstitial porosity, ϵ_e, for liquid–solid fluidized bed systems as

$$u = u_i \epsilon_e^n \quad (1)$$

where

$$\log u_i = \log(u_t) - \frac{d_p}{D} \quad (2)$$

and n is the bed expansion index, u_i is the terminal velocity of a homogeneous, rigid, spherical particle in an infinite medium, u_t is the particle terminal velocity, d_p is the particle diameter, and D is the column diameter [50]. The bed expansion index is a function of the terminal settling Reynolds number, N_{Ret}, particle diameter, and column diameter

$$n = 4.65 + 20\left(\frac{d_p}{D}\right) \quad (3)$$

for $N_{Ret} < 0.2$ [51]. The range of N_{Ret} for these studies was 0.002–0.03 (calculated using the batch average particle diameter).

2.4. Determination of residence time distributions

Residence time distribution (RTD) studies were performed using a tracer stimulus method [4,47] to assess the degree of liquid phase dispersion as a function of the degree of bed expansion. RTD studies were performed using nitrite, BSA and methylene blue (each under non-binding conditions) using a pulse input for the nitrite and a step input for the BSA and methylene blue. The UV absorbance of nitrite was measured at 254 nm and both BSA and methylene blue at 280 nm. The settled bed height was 2.1 cm for the nitrite RTD studies and 2.3 cm for both the BSA and methylene blue RTD studies.

For the nitrite RTD studies, a 0.5 ml pulse of 1 *M* sodium nitrite (Sigma) in equilibration buffer {100 m*M* sodium fluoride (Sigma, ACS reagent), 50 m*M* MES [2-(*N*-morpholino)ethanesulfonic acid] (Sigma) pH 5.5} was injected into the flow system using a 0.8 mm I.D. PTFE multiport sample injection valve (Rheodyne model 5020, Chrom Tech) placed between the fluid reservoir and the pump. The liquid volume of the tubing and connectors before the detector was 2.4 ml. The liquid volumes of the standard 4° and conical 45° flow distributors were 0.5 and 1.5 ml, respectively. The sodium nitrite was shown not to interact with the zirconia surface in the presence of fluoride by comparing the retention times of repeated injections of 1 *M* sodium nitrite in equilibration buffers containing 100 m*M* and 200 m*M* sodium fluoride (data not shown).

The sodium nitrite RTD experiments measured the relative degree of dispersion in the system tubing alone (with the column bypassed by connecting the column inlet directly to the column outlet) and for the entire system (tubing, fittings, bed, particles, detector) as a function of bed expansion. The system dispersion was also measured as a function of column inlet flow distributor design by placing the hydraulic header on top of the PTFE ring (see Fig. 1A) with the screen in place but without the particles. The system dispersion using the two inlet flow geometries was also compared at different bed expansions.

For all nitrite RTD studies, the particle bed was saturated with the equilibration buffer and then expanded to the appropriate height. The expanded bed height was allowed to stabilize for 10 min before the nitrite tracer was injected. Two successive injections of nitrite were then made at each bed expansion (for both flow distributors).

The BSA RTD experiments measured the system dispersion (tubing, fittings, bed of particles, and

detector) as a function of bed expansion and hydraulic header position. The mixing caused by the 1.0 cm long (4.9 ml) liquid space above the expanded bed surface was measured as a function of bed expansion by comparing RTDs obtained using two hydraulic header positions: 1.00±0.05 cm and 0.10±0.05 cm above the expanded bed surface. The conical 45° flow distributor was used for all BSA RTD experiments. The system liquid volume includes the tubing and connector volume before the detector, 2.7 ml, the volume of the conical 45° flow distributor, 1.5 ml, and the volume of liquid in the column assuming particles with an ϵ_i of 0.50 (Table 1) and assuming an ϵ_e of 0.4 for the settled bed of particles.

For the BSA RTD studies, the surface of the bare zirconia particles was modified by adsorption of fluoride from the mobile phase elution buffer [50 m*M* MES, 100 m*M* sodium fluoride and 750 m*M* sodium sulfate, anhydrous (Mallinkrodt) pH 5.5]. The RTD of 4 mg BSA/ml was studied under non-binding conditions using elution buffer. The BSA RTD breakthrough procedure consisted of first washing with 100 ml of 0.25 *M* sodium hydroxide, washing with the elution buffer until the effluent pH returned to pH 5.5±0.2, washing with elution buffer containing BSA until the column effluent BSA concentration equaled the column inlet BSA concentration, and finally washing the column with double distilled water. Adsorbed fluoride was stripped during column washing with 0.25 *M* sodium hydroxide but the surface was regenerated by washing the column with elution buffer.

The BSA was shown not to appreciably bind to the zirconia surface in the presence of sodium fluoride and sodium sulfate by comparing the breakthrough times of 4 mg/ml BSA dissolved in three buffers: elution buffer, buffer containing 75 m*M* MES, 150 m*M* sodium fluoride, with 1.125 *M* sodium sulfate, and buffer containing 100 m*M* MES, 200 m*M* sodium fluoride with 1.50 *M* sodium sulfate. The breakthrough times of BSA dissolved in the three buffers were equal within experimental error. The BSA was also shown not to bind to the fluoride-modified zirconia surface by comparing the area above the BSA breakthrough curve (BSA dissolved in elution buffer) with the area under the curve of an immediately following washing step with elution buffer (not containing BSA) which were equal within experimental error.

For the methylene blue RTD experiments, the surface of the bare zirconia was also modified by adsorption of fluoride. A solution of $2.8 \cdot 10^{-5}$ *M* methylene blue in the elution buffer was used. All expanded bed experiments used the conical 45°C flow distributer and the hydraulic header was positioned 1.00±0.05 cm above the expanded bed surface. The methylene blue RTD experiments were designed to visualize the flow behavior within the particle bed and within the 4.9 ml liquid space above the expanded bed surface. The methylene blue breakthrough procedure was the same as that used for the BSA RTD studies. The methylene blue (dissolved in the elution buffer) did not bind to the zirconia surface.

2.5. Determination of BSA dynamic binding capacity

BSA was adsorbed onto fluoride-adsorbed zirconia [38] from an initial concentration of 4 mg BSA/ml in equilibration buffer. BSA was eluted by a step increase in ionic strength using the elution buffer. Each BSA breakthrough procedure consisted of first washing with 100 ml of 0.1–0.25 *M* sodium hydroxide, washing with equilibration buffer until the pH returned to pH 5.5±0.2, followed by BSA loading (equilibration buffer containing BSA), washing with equilibration buffer, eluting adsorbed BSA with elution buffer, cleaning with 0.25 *M* sodium hydroxide, and rinsing with double distilled water until the effluent pH was within 0.5 pH units of the water.

Triplicate BSA binding breakthrough curves were obtained in a settled bed and at 2×, 2.5× and 3× bed expansions. Protein adsorption breakthrough profiles were generated either by protein loading while gradually increasing the flow-rate and expanding the bed to its final porosity over a period of 2.0–2.5 min, or protein loading after establishing a stable and fully expanded bed. The settled bed height for the protein adsorption studies was 2.3 cm.

Dynamic binding capacity (DBC) was calculated from BSA UV adsorption breakthrough curves as

DBC
$= [C_0(\text{Effluent volume corrected for system liquid volume})]/V_0$ (4)

where V_0 denotes the empty column volume for the settled bed of particles. When column effluent volume was not corrected for system liquid volume, DBC was expressed as mg BSA in the system (bound BSA and unbound BSA in the liquid phase)/ml of settled bed. As the degree of bed expansion was increased, the system liquid volume increased and the mass of protein in the system also increased. Therefore it was necessary to correct for the system liquid volume when calculating the amount of BSA bound to the support when using the BSA UV adsorption breakthrough curves.

Three different methods were used to correct the column effluent volume for the system liquid volume: (1) the calculated system liquid volume was subtracted from the BSA adsorption breakthrough curves; (2) a regressed nitrite RTD breakthrough curve was subtracted from the BSA adsorption breakthrough curves; (3) a regressed BSA RTD breakthrough curve was subtracted from the BSA adsorption breakthrough curves. The calculated system liquid volume was determined by summing all the calculated volumes for the column and for each length of tubing before the UV detector. The R-Code software package [52] was used to obtain the regressed breakthrough curves at each bed expansion for the nitrite and BSA RTDs. The nitrite RTD breakthrough curves were obtained by integrating the nitrite RTD peaks. The system liquid volume was calculated assuming an ϵ_e of 0.4 and using an internal porosity, ϵ_i, of 0.50 (Table 1).

The DBC at 5% breakthrough ($C/C_0=0.05$) was also calculated using the graphical method of Geankoplis [46]

DBC at 5% breakthrough =

$$\frac{C_0}{V_0}\int_0^{V(\frac{C}{C_0}=0.05)}\left(1-\frac{C}{C_0}\right)dV \quad (5)$$

where V denotes the column effluent volume. Similarly, the total DBC was calculated using the graphical method of Geankoplis [46]

$$\text{Total DBC} = \frac{C_0}{V_0}\int_0^{V_\infty}\left(1-\frac{C}{C_0}\right)dV \quad (6)$$

2.6. Bed cleaning

Particles were routinely cleaned of adsorbed protein during bed expansion by flushing with three column volumes of 0.1 or 0.25 *M* sodium hydroxide. More vigorous cleaning of the particles was achieved by removing them from the column into a polypropylene flask with 250 ml of 0.5 *M* sodium hydroxide and shaking at 300 rpm at 50°C for 64 h. Between experiments, the bed of particles was saturated with double distilled water or the equilibration buffer.

Table 1
Characterization of zirconium oxide particles

	Batch 1	Batch 2	FBOM[a]
Mean diameter	54 μm	43 μm	
Particle diameter range	20–140 μm	25–104 μm	75–103 μm
Internal porosity	0.47±0.03	0.50±0.03	
Density using gravimetry	3.48±0.15 g/ml	3.33±0.15 g/ml	
Nitrogen sorptometry			
Surface area	21.7±0.2 m^2/g	21.22±0.2 m^2/g	32.53±0.22 m^2/g
Void volume	0.183±0.002 ml/g	0.193±0.002 ml/g	0.265 ml/g
Hydraulic pore diameter (4*V*/*A*)	338 Å	366 Å	328 Å
BET adsorption peak	516 Å	580 Å	500 Å
BET desorption peaks	292 Å, 310 Å	312 Å, 363 Å	310 Å
Internal porosity	0.51±0.02	0.53±0.02	0.60
Density	3.30±0.10 g/ml	3.22±0.09 g/ml	2.87 g/ml

[a] Synthesis described in Ref. [43].

3. Results

3.1. Synthesis, classification and characterization of porous zirconium oxide particles

Two batches of particles of approximately 50 μm mean diameter were synthesized and characterized (Table 1) by screening, nitrogen sorptometry, and SEM (Fig. 2). The average diameter of zirconium oxide particles after elutriation (determined by particle screening) and the average hydraulic pore diameter (determined by nitrogen sorptometry) varied only slightly from batch to batch (Table 1) and is similar to that of a related synthesis method recently reported for FBOM zirconium oxide particles [43]. Particles prepared by batch synthesis were generally spherical with only a few particles slightly flattened or indented. Determination of the effective particle density from weighing (in air and in water) agrees well with that calculated from nitrogen sorptometry (Table 1).

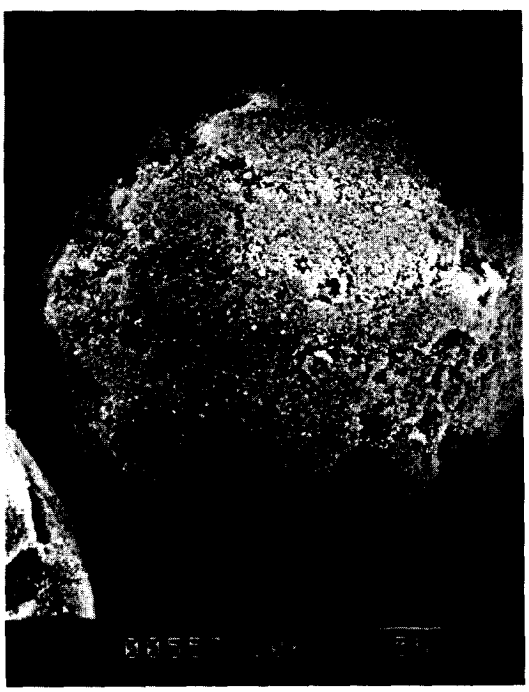

Fig. 2. Scanning electron micrograph of a zirconium oxide particle after classification by elutriation. Bar represents 5 μm.

3.2. Characterization of fluidization

The flow behavior of the porous zirconium oxide particles was characterized in double distilled water, equilibration buffer containing BSA and elution buffer containing BSA (Fig. 3). The bed expansion as a function of linear velocity curves in Fig. 3 have different slopes and intercepts which are caused by differences in the solution viscosities (Table 2). BSA adsorption studies and BSA RTD studies (under non-binding conditions) were carried out with particles at bed expansions of twice to triple the settled bed height (2–3× bed expansions) using corresponding linear flow velocities of 100–210 cm/h (BSA adsorption studies) and 60–140 cm/h (BSA RTD studies) (Fig. 3). Settled bed studies were carried out at a linear velocity of approximately 100 cm/h and 60 cm/h depending on the fluidizing liquid. Linear velocities were calculated as Q/A_{CS} where Q and A_{CS} are the volumetric flow-rate and the empty column cross-sectional area (πR^2), respectively.

The relationship between ϵ_e and u was found to agree well with the Richardson–Zaki relationship with $n=5.6$ indicating laminar flow [50,52,53] and a u_i value of 2.7–3.1 mm/s depending upon the particle batch. The experimentally determined value of u_i is consistent with that given by Stoke's law and the particle density (Table 1). The experimentally

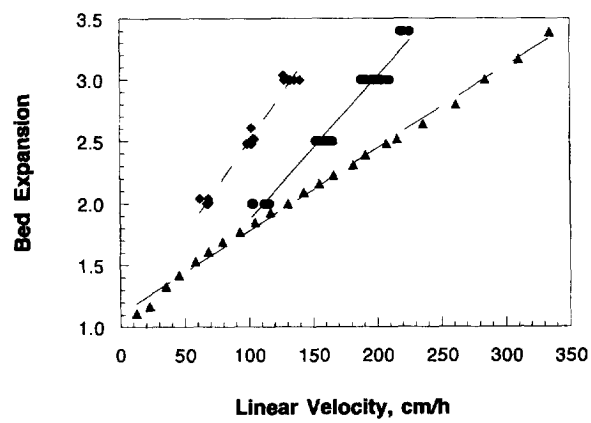

Fig. 3. Bed expansion as a function of linear velocity for zirconium oxide particles. Settled bed height, 2.3 cm with 2.5 cm I.D. column; (▲) double distilled water; (●) 4 mg/ml BSA in equilibration buffer; (♦) 4 mg/ml BSA in elution buffer.

Table 2
Characterization of fluidizing solutions

Solution	Viscosity, g/cm s	Density, g/ml
Equilibration buffer	0.011	1.00
Elution buffer	0.015	1.01
4 mg BSA/ml equilibration buffer	0.012	1.01
4 mg BSA/ml elution buffer	0.018	1.09

obtained value of n is higher than the value calculated from Eq. (3) ($n=4.7$) using the average particle diameter. However, this is consistent with other studies which have also reported larger values of n compared to the values predicted by Eq. (3) [14,48,50,54].

3.3. Residence time distribution and flow distributor design studies

RTDs for the system tubing alone and for the system without particles in the column were determined using the nitrite tracer (Fig. 4). The nitrite RTDs for the complete system (including the bed of particles) were measured as a function of bed expansion and flow distributors (Fig. 5A,B). The number of system liquid volumes was calculated as the effluent volume divided by the calculated system liquid volume. With particles in the column, bimodal peaks were observed using the 4° flow distributor (Fig. 5B) which were eliminated by using the conical 45° flow distributor. The nitrite RTD curves, were very reproducible and therefore replicate curves are not shown with the exception of the 2.5× expanded bed using the 4° flow distributor (Fig. 5B). This

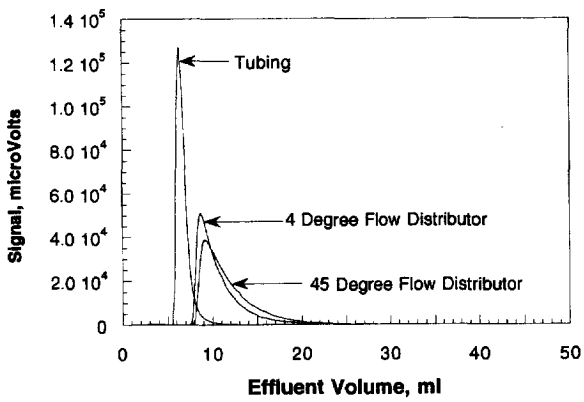

Fig. 4. Nitrite tracer residence time distributions as a function of flow distributor geometry without particles in the column using a flow-rate of 9.5 ml/min: tubing alone by connecting the column inlet to the column outlet; tubing and flow distributor with the hydraulic header directly on top of the PTFE ring with the screen placed between the distributor and the ring: standard 4° and conical 45° flow distributors.

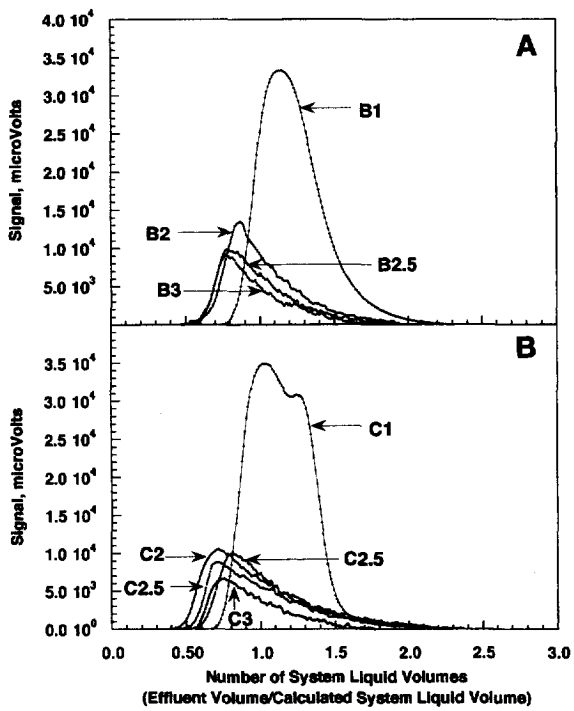

Fig. 5. Nitrite tracer residence time distributions as a function of flow distributor geometry with particles in the column. Settled bed height 2.1 cm. (A) Conical 45° flow distributor: settled bed flow-rate 9.5 ml/min; B2, 2× expansion (flow-rate 9.5 ml/min); B2.5, 2.5× expansion (flow-rate 13.5 ml/min); B3, 3× expansion (flow-rate 18.8 ml/min). (B) Standard 4° flow distributor: settled bed flow-rate 9.5 ml/min; C2, 2× expansion (flow-rate 9.5 ml/min); C2.5, 2.5× expansion (flow-rate 13.5 ml/min); C3, 3× expansion (flow-rate 18.8 ml/min).

indicates that once the bed is stably expanded, the flow behavior is constant.

While the residence time distributions for either flow distributor at constant flow-rate were sharp for the tubing alone (Fig. 4) and for a settled bed of particles using the conical 45° flow distributor (Fig. 5A), significant peak broadening and tailing was observed when the bed was expanded (Fig. 5A,B). All of the nitrite RTD peak fronts eluted from the column in less than one system liquid volume (measured at 5% of maximum peak height) indicating channeling. As the degree of bed expansion increased, the peak front eluted closer to one system liquid volume for the 4° flow distributor. In contrast, the degree of liquid channeling for the conical 45° flow distributor was not a function of bed expansion. There was significantly less liquid channeling in the settled bed than any of the expanded beds when using either flow distributor. The degree of liquid channeling was not significantly different between the two distributors for the 2.5× and 3× expanded beds but there was more liquid channeling for the 4° flow distributor for both the settled bed of particles and the 2× bed expansion.

There was no significant trend with degree of expansion in the number of system liquid volumes required to completely elute the nitrite tracer from the system for the experiments using the conical 45° flow distributor. The mean number of system liquid volumes required to completely elute the 0.5 ml of nitrite tracer from the system was 1.1±0.1 system liquid volumes indicating a significant amount of mixing in the column. For the 4° flow distributor, the number of system liquid volumes required to completely elute the tracer from the system for the 2× and 2.5× expanded beds is approximately twice that for the settled bed and 3× bed expansion. The 4° flow distributor caused more mixing in the 2× and 2.5× expanded beds than the conical 45° flow distributor. The 45° flow distributor caused more mixing in the settled bed than the 4° flow distributor. As a result of these nitrite RTD studies, BSA adsorption studies were completed using the 45° flow distributor.

The nitrite RTD peaks were analyzed to determine the number of ideal CSTRs (continually stirred tank reactors) in series that would give the same peak shape as the nitrite RTD peak [55]. As expected, the experimental peaks for all bed expansions were more highly tailed than the model predictions (data not shown).

Residence time distributions for the complete system (tubing, flow distributor and bed of particles) were also obtained as a function of bed expansion using BSA as a tracer under non-binding conditions. The degree of mixing caused by the 4.9 ml (1 cm high) of liquid volume above the expanded bed surface at all bed expansions was determined by comparing the BSA RTDs for two hydraulic header positions: 1.00±0.05 and 0.10±0.05 cm above the expanded bed surface (Fig. 6A,B).

While the BSA RTDs were sharp for a settled bed of particles, significant broadening of the breakthrough curve occurred upon expansion of the bed (Fig. 6A,B). All of the breakthrough curves eluted from the column in less than one system liquid volume indicating channeling. The degree of channeling was not a function of bed expansion for either hydraulic header position. However, the channeling was reduced for the settled bed of particles compared to all bed expansions regardless of the header position. The degree of liquid channeling was also not a function of hydraulic header position (Fig. 7A,B,C).

There was no significant trend in the protein RTD breakthrough curve widths as a function of bed expansion or hydraulic header position. Curve width was calculated as the number of system liquid volumes at 95% breakthrough ($C/C_0=0.95$) minus the number of system liquid volumes at 5% breakthrough. This method is equivalent to calculating the number of system liquid volumes required to completely elute the tracer from the system as determined by the nitrite RTD experiments. The average width (±1 S.D., one standard deviation) for all experiments was 1.2±0.1 system liquid volumes (Fig. 7A,B,C). A noticeable shoulder is observed in the breakthrough curves when the header was placed 1.00±0.05 cm above the expanded bed surface suggesting two flow regimes within the column caused by the 4.9 ml liquid space above the expanded bed surface. This behavior was eliminated by lowering the header to 0.10±0.05 cm above the expanded bed.

The nitrite and BSA RTD results indicated the presence of channeling of liquid through the bed of

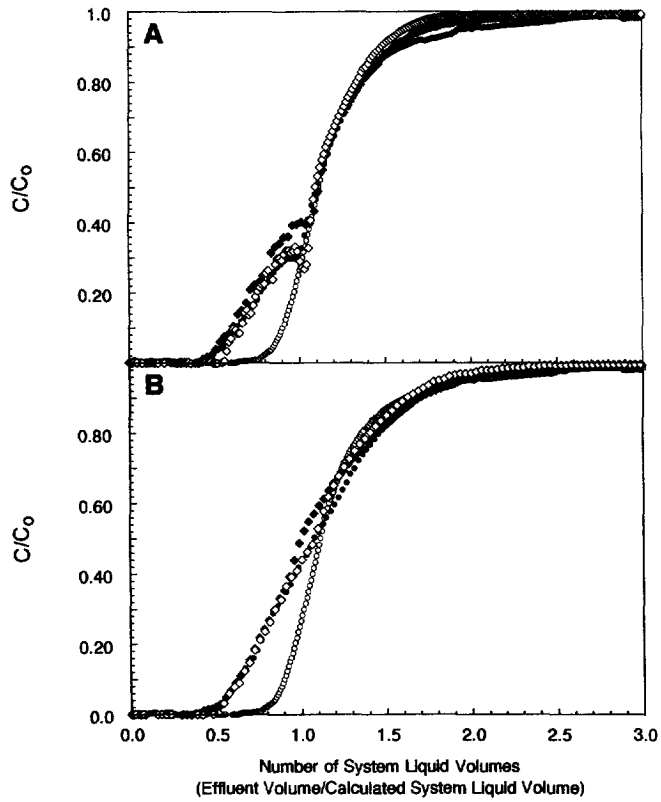

Fig. 6. BSA tracer residence time distributions as a function of bed expansion and hydraulic header position. Header placed on top of bed for settled bed experiments. Settled bed height 2.3 cm, conical 45° flow distributor. (○) Settled bed (flow-rate 6.0 ml/min); (●) 2× expansion (flow-rate 6.0 ml/min); (♦) 2.5× expansion (flow-rate 8.5 ml/min); (◇) 3× expansion (flow-rate 11.1 ml/min). Replicate curves not shown. (A) Hydraulic header positioned 1.00±0.05 cm above the surface of the expanded bed. (B) Hydraulic header positioned 0.10±0.05 cm above the surface of the expanded bed.

particles. Methylene blue was an effective tracer in order to visually confirm the channeling of liquid within the particle bed and within the 4.9 ml liquid space above the expanded bed surface. The methylene blue (in expanded beds) began eluting from the column in much less than one (~0.54) system liquid volume. The dye front exited the bed after a channel of blue dye exited the bed and the front was not sharp indicating mixing within the liquid above the bed. The blue dye was also visible along the column walls (within the expanded bed) after the front began exiting the bed suggesting channeling within the bed.

3.4. Determination of BSA dynamic binding capacity as a function of bed expansion

BSA adsorption from three replicates was compared between settled and expanded beds (Fig. 8). Adsorption and elution profiles for expanded beds were comparable to the settled bed (data not shown).

The total DBC of these dense zirconium oxide particles was constant for the packed bed and bed expansions up to three-fold (Fig. 9A). The total DBC was calculated from the breakthrough curves up to 98% saturation ($C/C_0=0.98$). The mean total DBC for all experiments was 42±2 mg BSA/ml of settled bed. There was no significant difference between the DBC at 5% breakthrough for the settled bed and 2× bed expansions and between the 2.5× and 3× bed expansions (Fig. 9B). The two methods used to calculate DBC at 5% breakthrough (Eqs. (4) and (5)) were in good agreement. In addition, there was no significant difference in the system liquid volume determination when correcting the effluent volume

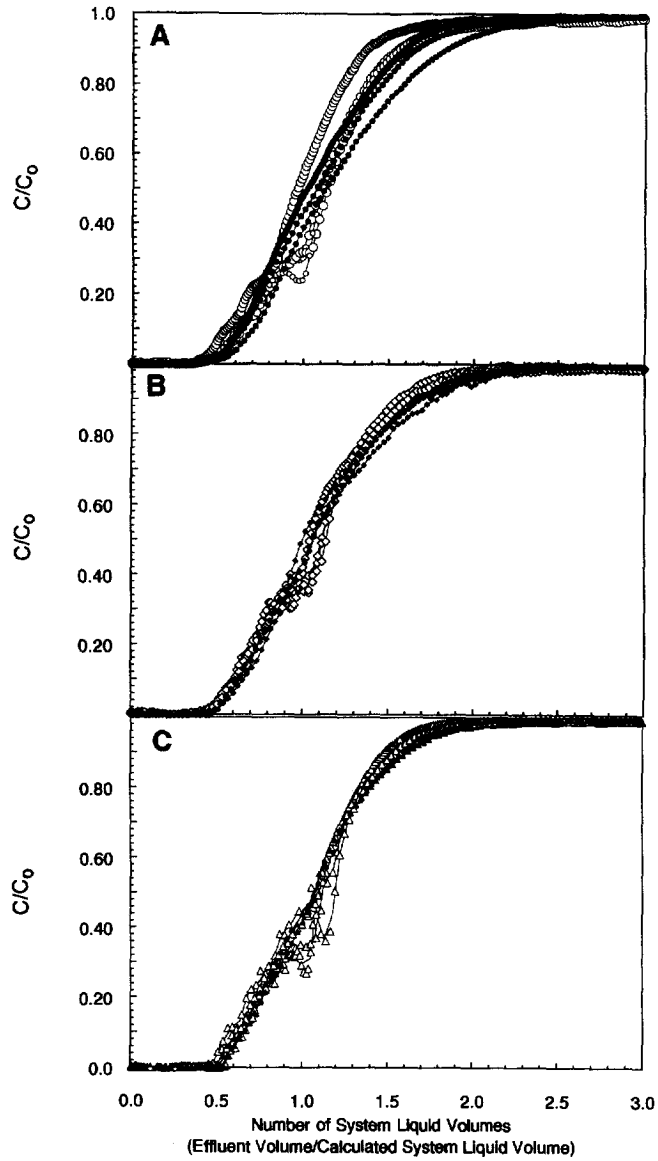

Fig. 7. BSA tracer residence time distributions as a function of bed expansion and hydraulic header position showing the data reproducibility. Conical 45° flow distributor. (A) 2× expansion (flow-rate 6.0 ml/min). (○) Hydraulic header 1.0 cm above expanded bed surface (four replicates shown); (●) hydraulic header 0.1 cm above expanded bed surface (three replicates shown). (B) 2.5× expansion (flow-rate 8.5 ml/min); (◇) hydraulic header 1.0 cm above expanded bed surface (four replicates shown); (◆) hydraulic header 0.1 cm above expanded bed surface (three replicates shown). (C) 3× expansion (flow-rate 11.1 ml/min). (△) hydraulic header 1.0 cm above expanded bed surface (four replicates shown); (▲) hydraulic header 0.1 cm above expanded bed surface (two replicates shown).

for the system liquid volume in Eq. (4). The DBC of BSA at 5% breakthrough was the same for a two-fold expanded bed as for a settled bed (22±2 mg BSA/ml of settled bed), though it decreased for higher bed expansions (15±1 mg BSA/ml settled bed). Furthermore, at 5% breakthrough, 54±4% of

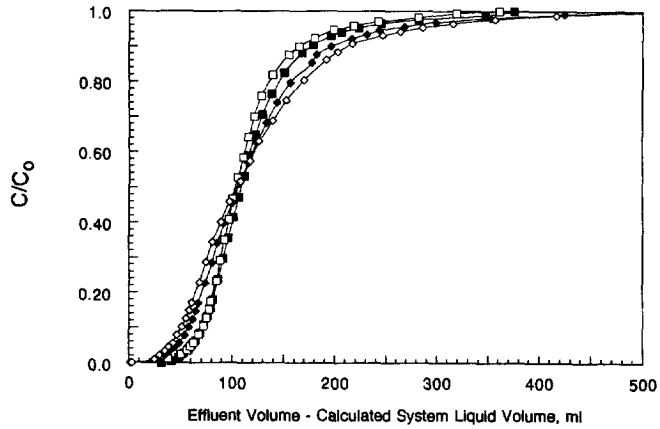

Fig. 8. BSA adsorption breakthrough curves as a function of bed expansion adjusted for increasing system liquid volume. Settled bed height 2.3 cm, conical 45° flow distributor, hydraulic header 1.0 cm above the expanded bed surface. (■) Settled bed (flow-rate 9.0 ml/min); (□) 2× expansion (flow-rate 9.5 ml/min); (♦) 2.5× expansion (flow-rate 13.0 ml/min); (◇) 3× expansion (flow-rate 16.3 ml/min). Replicate curves not shown.

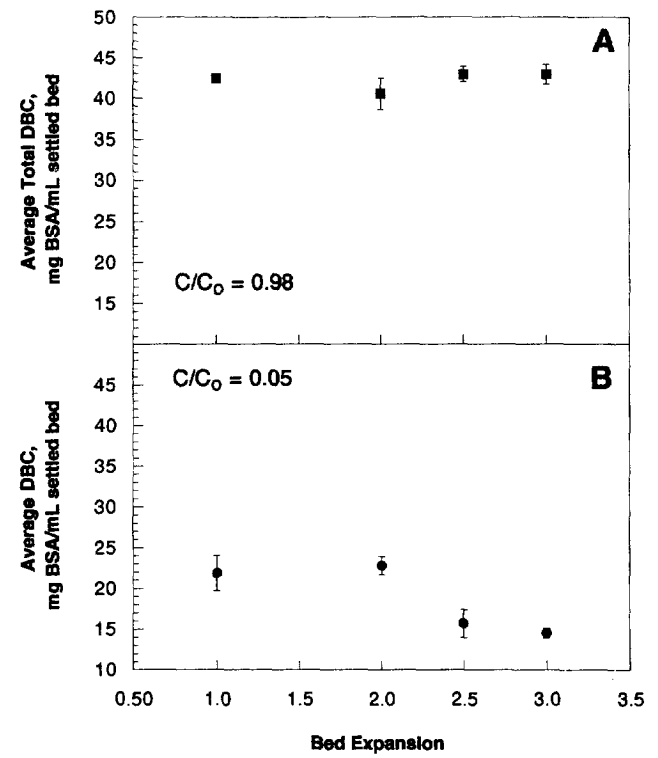

Fig. 9. Dynamic binding capacity of BSA on fluoride-adsorbed zirconium oxide particles as a function of bed expansion. Averages calculated from triplicate determinations; error bars represent one standard deviation. Conical 45° flow distributor. (A) Average total dynamic binding capacity, $C/C_0=0.98$. (B) Average dynamic binding capacity at $C/C_0=0.05$.

the total DBC was utilized for the two-fold expanded bed and settled bed and 35±4% was utilized for the 2.5× and 3× bed expansions.

This trend in 5% DBC as a function of bed expansion was observed with both BSA loading methods: gradually expanding the bed to full expansion during BSA loading and loading after full bed expansion is reached. This is because the time to fully expand the bed when switching from equilibration buffer to equilibration buffer containing BSA (1.9–2.7 min) was approximately one third of the time to 1% BSA breakthrough depending on fluidization velocity. BSA elution at constant flow-rate was consistently observed as a narrow peak.

3.5. Performance of porous zirconium oxide particles after repeated cleaning

Repeated cycles of BSA binding, elution and column cleaning with sodium hydroxide did not cause particle fracture or generation of fines over a nine month period of particle evaluation. During this time period, the particles were exposed to over 500 column volumes of sodium hydroxide. No bacterial growth inhibitor was needed for routine storage of the column at ambient temperature due to the presence of fluoride in the equilibration buffer. The particle size and distribution remained constant over one year of repeated adsorption/desorption and base cleaning cycles.

Protein adsorption studies using the same column of particles over an 8 month period revealed two factors that caused a dramatic decrease in the BSA DBC: poor inlet distributor design [14] and insufficient cleaning. The location of the retaining ring on the initial screen design (Fig. 1B) resulted in generation of small fluid jets at the base of the bed. These jets caused a reduction in DBC and were eliminated by using the design shown in Fig. 1A. Repetitive cleaning of the column with 0.1 *M* sodium hydroxide was not sufficient resulting in particle clumping. Frit clogging decreased the DBC by approximately 50% (data not shown). Clumped particles could be cleaned and dispersed by washing with 0.25–0.50 *M* sodium hydroxide with shaking at 50°C. This restored the BSA DBC to the original level. The dynamic binding capacity at a 2× bed expansion observed on the initial determinations was equivalent to that measured at the end of eight months of column use and after the 0.5 *M* sodium hydroxide wash with shaking at 50°C.

4. Discussion

This study confirms that dense porous zirconium oxide particles are useful for protein adsorption in shallow fluidized beds. These particles have a specific gravity of 3.2–3.3 g/ml a mean particle size of ~50 μm. The particle shape was primarily spherical, though some particles had indentations or were slightly ellipsoidal in contrast to the many types of angular particles whose properties have been studied in expanded beds [14]. At least 70% of the pores are sufficiently large for BSA adsorption. Stable expanded beds of particles were achieved using linear velocities from 100 to 210 cm/h which is much higher than could be achieved in shallow beds with similarly sized, but lower density polymeric particles [14].

The terminal velocity of these particles calculated from Stoke's law was 2.5–3.9 mm/s (depending on the batch) using water at 25°C as the fluidizing liquid. This is considerably faster than the calculated terminal velocity of 0.7 mm/s [4] for the 45–165 μm agarose matrix particles (Q-Sepharose Fast Flow, Pharmacia Biotech). It is comparable to that (3.6 mm/s) for the similarly sized (70 μm) perfluoropolymer adsorbents and is greater that the value of u_i reported for most silica particles and comparable to 63–100 μm Fractosil Si1000 particles [11,13,14] which achieve a high density at the expense of losing porosity. The terminal velocity of the zirconium oxide particles is also comparable to that for the much larger 206 μm (mean particle diameter) quartz-containing agarose particles (Streamline, Pharmacia Biotech). And it is smaller than that (22.4 mm/s) of the dense (2.2 g/ml), non-spherical and much larger 200 μm (mean particle diameter) controlled pore glass particles [17].

Though significant channeling and mixing occurred in the expanded beds using the small model column with the conical 45° flow distributor, the degree of liquid channeling was not so severe as to limit evaluation of particle performance. As expected, expanded bed stability was improved by

changing the flow distributor design (Fig. 1A). Increasing the ratio of settled bed height to column diameter would also likely improve expanded bed stability and increase DBC at high fluidization velocity due to a reduction in the effects of column inlet turbulence [18].

The RTD results suggest that the observed DBC at 5% breakthrough should be larger for a settled bed than for an expanded bed and it should not be dependent on the degree of bed expansion. However, this is not the case. The DBC for the settled bed and 2× bed expansion are the same but it is smaller for the 2.5× and 3× bed expansions. These discrepancies may arise from nonlinear BSA adsorption (e.g., protein overloading), axial dispersion in the bed, and/or stratification of the particles during fluidization. We are currently investigating the dominant mechanisms that result in this unexpected DBC behavior as a function of bed expansion.

Though significant peak broadening occurred during adsorption at 2×, 2.5× and 3× bed expansions, BSA elution (by altering the ionic strength at a constant flow-rate) was rapid and peaks were sharp and reproducible. This elution method may offer advantages for large scale protein capture in contrast to stopping flow and settling the bed and elution by reversing flow direction which is used for less dense and larger diameter expanded-bed adsorbents [8,9].

The method used in this study to calculate the amount of protein adsorbed to the particles by correcting the column effluent volume for the increasing system liquid volume with increasing bed expansion (i.e., as ϵ_e is increased) has not been previously reported. If BSA adsorption data are not corrected for the additional system liquid volume in expanded beds, the values of DBC at 5% breakthrough will be inflated. Both system liquid volume and flow behavior vary as a function of bed expansion.

BSA binding capacities comparable to larger polymeric particles with large settled bed height to diameter ratios [8] can be achieved at very high liquid velocities (>100 cm/h) even with a shallow bed of 43 μm or 54 μm zirconium particles. The use of small porous zirconia particles may allow fluidization at a velocity high enough to reach optimum expansion to minimize dispersion and separation of the adsorbent from entrained solids but with a reduced characteristic diffusion length within the adsorbent compared to larger (100–400 μm) and less dense polymeric particles.

The results reported here confirm that the choice of a dense, cleanable adsorbent for expanded bed protein adsorption can significantly effect bed stability, protein dynamic binding capacity, and protein elution at high fluid velocity. Evaluation of the fluidization of porous zirconium oxide particles for protein adsorption using BSA adsorption to fluoride-adsorbed zirconia over a period of twelve months indicates that these ceramic particles may be more stable than silica or polymeric ion-exchange particles in expanded beds [9,14]. Unless the flow distributor or the particles were insufficiently cleaned, BSA DBC was unchanged over a period of greater than 8 months with particles exposed to over 500 column volumes of sodium hydroxide.

The use of very dense particles for rapid protein adsorption at high fluid velocities and rapid protein elution at constant velocity without bed settling can significantly reduce column cycle time (equilibration, loading to breakthrough, washing, protein elution, cleaning) and may result in a significant productivity advantage for rapid concentration of labile proteins from large volumes of fluids. These very dense zirconia particles may also be especially useful for adsorption of proteins from high density and/or high viscosity fluids.

5. Abbreviations

A_{CS}	Column cross-sectional area based on column inner radius
BSA	Bovine serum albumin
C	Bulk solute concentration
C_0	Column inlet solute concentration
CSTR	Continually stirred tank reactor
D	Column inner diameter
d_p	Adsorbent particle diameter
DBC	Dynamic binding capacity
H	Bed height
LPS	Lipopolysaccharide
MES	2-(*N*-Morpholino)ethane sulfonic acid
MSFB	Magnetically stabilized fluidized bed
N_{Ret}	Particle Reynolds number
Q	Volumetric flow-rate

RTD	Residence time distributon
SEM	Scanning electron microscopy
u	Superficial liquid velocity
u_t	Particle terminal velocity
u_i	Terminal velocity of a rigid, spherical particle in infinite medium
V	Column effluent volume
V_0	Empty container fluid volume
ϵ_e	Interstitial porosity
ϵ_i	Internal porosity

Acknowledgments

The authors would like to acknowledge the insight and advice of Professor P.W. Carr, the technical support of David Reeder for assistance in particle characterization, and Carol Tolppi for preliminary expanded bed experiments. The authors would also like to acknowledge financial support for portions of this work from the National Science Foundation (CHE 917029), the National Institutes of Health (GM 45988), and the Biological Process Technology Institute.

References

[1] C.H. Lochmüller, C.S. Ronsick, L.S. Wigman, Prep. Chromatogr. 1 (1988) 93.
[2] N.M. Drager, H.A. Chase, in: D.L. Pyle (Ed.), Separations for Biotechnology 2, Elsevier, Barking, 1990, p. 325.
[3] N.M. Draeger, H.A. Chase, in: Advances in Separation Processes (Int. Chem. Eng. Journ.), Symp. Ser. 118 (1990) 161.
[4] N.M. Draeger, H.A. Chase, Trans. Int. Chem. Eng. 69 (1991) 45.
[5] Y.K. Chang, H.A. Chase, Biotechnol. Bioeng. 49 (1996) 204.
[6] N.M. Draeger, H.A. Chase, Bioseparation 2 (1991) 67.
[7] P. Hedman, A.-K. Barnfield Frej, in: M.R. Ladisch, A. Bose (Eds.) Harnessing Biotechnology for the 21st Century, ACS Conference Proceedings Series, American Chemical Society, Washington DC, 1992, p. 271.
[8] H.A. Chase, N.M. Draeger, J. Chromatogr. 597 (1992) 129.
[9] H.A. Chase, TIBTECH 12 (1994) 296.
[10] M. Hansson, S. Ståhl, R. Hjorth, M. Uhlen, T. Moks, Bio/Technology 12 (1994) 285.
[11] G.E. McCreath, H.A. Chase, R.O. Owen, C.R. Lowe, Biotechnol. Bioeng. 48 (1995) 341.
[12] Y.K. Chang, G.E. McCreath, H.A. Chase, Biotechnol. Bioeng. 48 (1995) 355.
[13] R.O. Owen, H.A. Chase, J. Chromatogr. A 757 (1997) 41.
[14] G.M.S. Finette, Q-M. Mao, M.T.W. Hearn, J. Chromatogr. A 743 (1996) 57.
[15] N.B. Gibson, A. Lydiatt, in: J.F. Kennedy, G.O. Phillips, P.A. Williams (Eds.). Cellulosics: Materials for Selective Separations and Other Technologies, Ellis Horwood, New York, 1993, p. 55.
[16] G.R. Gilchrist, M.T. Burns, A. Lydiatt, in: D.L. Pyle (Ed.), Separation for Biotechnology, Elsevier, Oxford, 1994, p. 186.
[17] J. Thömmes, M. Halfar, S. Lenz, M.-R. Kula, Biotechnol. Bioeng. 45 (1995) 205.
[18] J. Thömmes, M. Weiher, A. Karau, M.-R. Kula, Biotechnol. Bioeng. 48 (1995) 367.
[19] P.W. Carr, J.A. Blackwell, T.P. Weber, W.A. Schafer, M.P. Rigney, in: Cs. Horváth, L.S. Ettre (Eds.), Chromatography in Biotechnology, ACS Symposium Series, No. 529, Washington, DC, 1993, p. 146.
[20] J. Nawrocki, M.P. Rigney, A. McCormick, P.W. Carr, J. Chromatogr. A 657 (1993) 229.
[21] J. Nawrocki, C.J. Dunlap, P.W.Carr, J.A. Blackwell, Biotechnol. Prog. 10 (1994) 561.
[22] A. Tripodi, A. Nowotny, Ann. N.Y. Acad. Sci. 133 (1966) 604.
[23] M. Niwa, K.C. Milner, E. Ribi, J.A. Rudbach, J. Bacteriol. 97 (1969) 1069.
[24] Pharmacia Downstream News, Views for Process Biotechnologists, No. 2, Pharmacia, Piscataway, NJ, 1986.
[25] C.P. Prior, in: C. Ho, D.I.C. Wang (Editors), Animal Cell Bioreactors, Butterworth-Heinemann, 1991, Ch. 17, p. 445.
[26] A.R. Barry, R. Chojnacki, BioPharm 7 (8) (1994) 43.
[27] A. Jungbauer, J. Chromatogr. 639 (1993) 3.
[28] M. Weary, F. Pearson, BioPharm 1 (4) (1988) 22.
[29] J.C. Janson, T. Petterson, in: G. Ganetos, P.E. Barker (Eds.), Preparative and Production Scale Chromatography, Marcel Dekker, New York, 1992, Ch. 22, p. 559.
[30] N. Adner, G. Sofer, BioPharm 7(3) (1994) 44.
[31] A. Jungbauer, H.P. Lettner, BioPharm 7(5) (1994) 46.
[32] A. Jungbauer, H.P. Lettner, L. Guerrier, E. Boschetti, BioPharm 7(6) (1994) 41.
[33] R.J. Seeley, H. Dwight, H.H. Fry, S.R. Rudge, G.F. Slaff, BioPharm 7(7) (1994) 41.
[34] R.W. Kozak, C.N. Durfer, C.L. Scribner, Cytotechnology 9 (1992) 203.
[35] WHO Study Group, Acceptability of All Substances for Production of Biologicals (Technical Report Series 747) World Health Organization, Geneva, 1987.
[36] P. Girot, Y. Moroux, X.P. Duteil, C. Nguyen, E. Boschetti, J. Chromatogr. 510 (1990) 213.
[37] E. Boschetti, P. Girot, L. Guerrier, J. Chromatogr. 523 (1990) 35.
[38] J.A. Blackwell, P.W. Carr, J. Chromatogr. 549 (1991) 59.
[39] P.R. Levison, in: G. Ganetos, P.E. Barker (Eds.), Preparative and Production Scale Chromatography, Marcel Dekker, New York, 1992, Ch. 25, p. 617.
[40] P.H. Morton, A. Lydiatt, in: J.F. Kennedy, G.O. Phillips, P.A. Williams (Eds.), Cellulosics: Materials for Selective Separations and Other Technologies, Ellis Horwood, New York, 1993.

[41] P.W. Carr, E.F. Funkenbush, M.P. Rigney, P.A. Coleman, D.A. Hanggi, W.A. Schafer, US Pat. 5 015 373, 1991.
[42] E.F. Funkenbush, P.W. Carr, D.A. Hanggi, T.P. Weber, US Pat. 5 108 597, 1992.
[43] M.J. Robichaud, A.N. Sathyagal, P.W. Carr, A.V. McCormick, M.C. Flickinger, Sep. Sci. Technol. (in press).
[44] S. Brunauer, P.H. Emmett, E. Teller, J. Am. Chem. Soc. 60 (1938) 309.
[45] S.J. Gregg, K.S.W. Sing, Adsorption Surface and Porosity, Academic Press, New York, 1982.
[46] C.J. Geankoplis, Transport Processes and Unit Operations, Prentice Hall, New York, 1993, p. 700.
[47] P. Wnukowski, A. Lindgren, Recovery of Biological Products IV, Engineering Foundation Conference, Interlaken, 1992.
[48] J.F. Richardson, W.N. Zaki, Trans. Inst. Chem. Eng. 32 (1954) 35.
[49] C.W. Macosko, Rheology: Principles, Measurements and Applications, VCH, Weinheim, 1995.
[50] G. Dasari, I. Prince, M.T.W. Hearn, J. Chromatogr. 631 (1993) 115.
[51] J.F. Davidson, D. Harrison (Eds.), Fluidization, Academic Press, London, 1971.
[52] R.D. Cook, S. Weisberg, An Introduction to Regression Graphics, Wiley, New York, 1994.
[53] Y.S. Chong, D.A. Ratkowsky, N. Epstein, Powder Technol. 23 (1979) 55.
[54] R. Jottrand, J. Appl. Chem. (London), 2 Suppl. Issue I, (1952) S17–S26.
[55] H.S. Fogler, Elements of Chemical Reaction Engineering, 2nd ed., Prentice-Hall, Englewood Cliffs, NJ, 1992.